High resolution crystal structure of rat long chain hydroxy acid oxidase in complex with the inhibitor 4-carboxy-5-[(4-chlorophenyl)sulfanyl]-1, 2, 3-thiadiazole. Implications for...

ARTICLE *in* BIOCHIMIE · FEBRUARY 2012

Impact Factor: 2.96 · DOI: 10.1016/j.biochi.2012.02.003 · Source: PubMed

Biochimie 94 (2012) 1172–1179

Contents lists available at SciVerse ScienceDirect

Biochimie

journal homepage: www.elsevier.com/locate/biochi

Research paper

High resolution crystal structure of rat long chain hydroxy acid oxidase in complex with the inhibitor 4-carboxy-5-[(4-chlorophenyl)sulfanyl]-1, 2, 3-thiadiazole. Implications for inhibitor specificity and drug design

Zhi-wei Chen [a], Caroline Vignaud [b], Adil Jaafar [c], Bernard Lévy [c], Françoise Guéritte [d], Daniel Guénard [d], Florence Lederer [c], F. Scott Mathews [a,*]

[a] Department of Biochemistry and Molecular Biophysics, Washington University School of Medicine, 660 South Euclid Avenue, St Louis, MO 63110, USA
[b] Laboratoire d'Enzymologie et Biochimie Structurales, CNRS FRE 2930, Gif-sur-Yvette, France
[c] Laboratoire de Chimie Physique, CNRS UMR 8000, Université Paris-Sud, Orsay, France
[d] Institut de Chimie des Substances Naturelles, CNRS UPR 2301, Gif-sur-Yvette, France

ARTICLE INFO

Article history:
Received 14 December 2011
Accepted 2 February 2012
Available online 9 February 2012

Keywords:
Crystal structure
Flavoprotein
Homology
Hydrogen bond
Long chain hydroxy acid oxidase
Inhibitor

ABSTRACT

Long chain hydroxy acid oxidase (LCHAO) is responsible for the formation of methylguanidine, a toxic compound with elevated serum levels in patients with chronic renal failure. Its isozyme glycolate oxidase (GOX), has a role in the formation of oxalate, which can lead to pathological deposits of calcium oxalate, in particular in the disease primary hyperoxaluria. Inhibitors of these two enzymes may have therapeutic value. These enzymes are the only human members of the family of FMN-dependent L-2-hydroxy acid-oxidizing enzymes, with yeast flavocytochrome b_2 (Fcb2) among its well studied members. We screened a chemical library for inhibitors, using in parallel rat LCHAO, human GOX and the Fcb2 flavodehydrogenase domain (FDH). Among the hits was an inhibitor, CCPST, with an IC_{50} in the micromolar range for all three enzymes. We report here the crystal structure of a complex between this compound and LCHAO at 1.3 Å resolution. In comparison with a lower resolution structure of this enzyme, binding of the inhibitor induces a conformational change in part of the TIM barrel loop 4, as well as protonation of the active site histidine. The CCPST interactions are compared with those it forms with human GOX and those formed by two other inhibitors with human GOX and spinach GOX. These compounds differ from CCPST in having the sulfur replaced with a nitrogen in the five-membered ring as well as different hydrophobic substituents. The possible reason for the ~100-fold difference in affinity between these two series of inhibitors is discussed. The present results indicate that specificity is an issue in the quest for therapeutic inhibitors of either LCHAO or GOX, but they may give leads for this quest.

1. Introduction

Long chain hydroxy acid oxidase (LCHAO) is a peroxisomal enzyme found essentially in liver and kidney. Its physiological function is not clearly established. It was first described as an L-amino acid oxidase, and subsequently found more active on L-2-hydroxy acids [1,2]. In the course of time, it was found capable of oxidizing a variety of compounds such as thyroxine [3], nephrotoxic cysteine conjugates such as S-(1,2-dichlorovinyl)-L-cysteine [4,5] and thiol-glyoxylate adducts [6,7]. LCHAO was later identified as the enzyme that oxidizes creatol with formation of methylguanidine in rat kidney [8,9]. Methylguanidine is a toxic compound with elevated serum levels in patients with chronic renal failure [10,11]. Creatol (hydroxy creatinine, or 2-amino-5-hydroxy-1-methyl-4(5H)imidazolone) (Fig. 1), which is not a 2-hydroxy acid, is spontaneously formed from creatinine by reactive oxygen species, which are elevated in uremic kidneys [12,13]. One may thus wonder if LCHAO inhibitors could be included in the treatment of uremic patients.

Abbreviations: AGT, alanine–glyoxylate transaminase; CCPST, 4-carboxy-5-(4-chlorophenyl)sulfanyl-1, 2, 3-thiadiazole; CDST, 4-carboxy-5-dodecylsulfanyl-1,2,3-triazole; DCIP, dichlorophenol indophenol; Fcb2, flavocytochrome b_2; FDH, flavodehydrogenase domain of Fcb2; hGOX, human glycolate oxidase; sGOX, spinach glycolate oxidase; GRHPR, glyoxylate reductase–hydroxypyruvate reductase; LCHAO, rat long chain hydroxy acid oxidase; TACA, 4-carboxy- 5-(1-pentyl) hexylsulfanyl-1,2,3-triazole.

* Corresponding author. Tel.: +1 314 362 1080; fax: +1 314 362 7183.
E-mail address: mathews@biochem.wustl.edu (F.S. Mathews).

0300-9084/$ – see front matter © 2012 Elsevier Masson SAS. All rights reserved.
doi:10.1016/j.biochi.2012.02.003

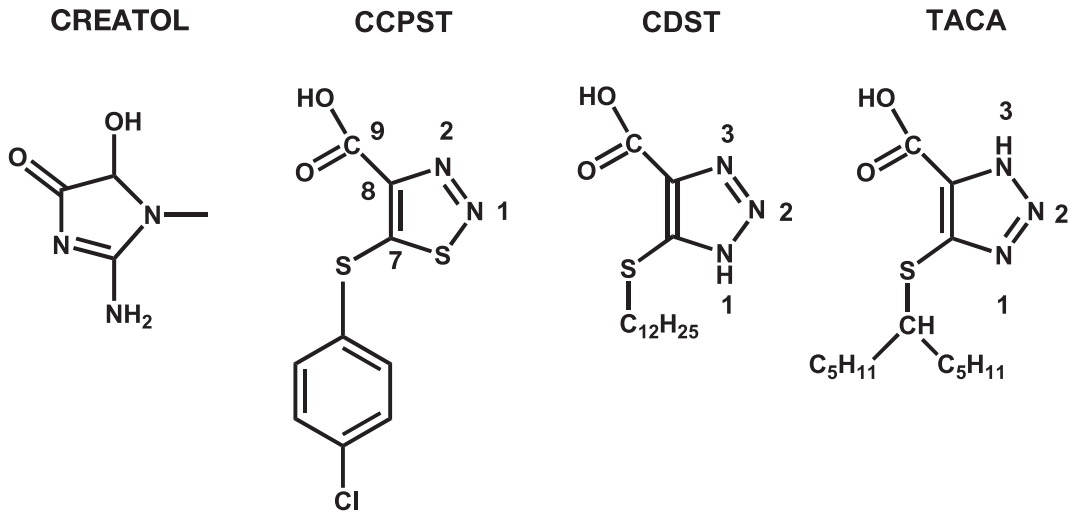

Fig. 1. Chemical structures of creatol, CCPST, CDST and TACA. The structure of CDST is represented with a proton on N1, as in [21], and that of TACA with the proton on N3, as in [26] (see discussion).

LCHAO (EC1.1.3.15, isozyme B) is an isozyme of short-chain hydroxy acid oxidase, better known as glycolate oxidase (GOX) (EC1.1.3.15, isozyme A). The latter oxidizes glycolate to glyoxylate, which is detoxified in the peroxisome by alanine–glyoxylate transaminase (AGT) or in the cytosol by glyoxylate reductase–hydroxypyruvate reductase (GRHPR). Glyoxylate can also be oxidized to oxalate, which is normally eliminated by the kidney. But, when produced in excess, oxalate can lead to pathological deposits of insoluble calcium oxalate. The severe genetic conditions primary hyperoxalurias type I and II result from deficiencies of AGT and GRHPR respectively [14]. It has been proposed that GOX inhibitors might be useful in the treatment of primary hyperoxaluria [15].

The human LCHAO and GOX genes, as well as that of the rat LCHAO have been cloned [16–18] and the respective recombinant proteins expressed. The crystal structure of rat LCHAO has been determined at 2.3 Å resolution [19]. It shows a TIM barrel fold, as do the other members of the family of FMN-dependent L-2-hydroxy acid-oxidizing enzymes, glycolate oxidase [20,21], lactate oxidase and lactate monooxygenase [22,23], mandelate dehydrogenase [24] and flavocytochrome b_2 (Fcb2, a yeast L-lactate dehydrogenase) [25]. The catalytic active site residues on the FMN *si* face (two arginines, two tyrosines and a histidine) are all conserved, except for one of the tyrosines which is a phenylalanine in LCHAO.

We screened a chemical library for inhibitors of LCHAO, using in parallel hGOX and the flavodehydrogenase (FDH) domain of flavocytochrome b_2 (Fcb2). One of the hits inhibited the three enzymes with a K_d in the μM range. This compound, 4-carboxy-5-[(4-chlorophenyl)sulfanyl]-1, 2, 3-thiadiazole (CCPST) presents an overall similarity with TACA (Fig. 1), an inhibitor crystallized in complex with spinach GOX (sGOX) [26]. More recently, the human enzyme hGOX was crystallized with another inhibitor, CDST, which differs from TACA only by the sulfur hydrophobic substituent (Fig. 1) [21]. It appeared of interest to determine the structure of CCPST in complex with these enzymes in order to understand the reasons for its relative absence of specificity. The structure of hGOX in complex with CCPST is now published [27]. We present here the crystal structure at 1.3 Å resolution of rat LCHAO in complex with this same inhibitor. We compare it with the 2.3 Å resolution structure of LCHAO, having acetate from the mother liquors bound in the active site [19], with the 2.8 Å structure of the hGOX-CCPST complex, as well as with the structures of the hGOX-CDST and sGOX-TACA complexes.

2. Materials and methods

2.1. Enzymes and assays

Two forms of LCHAO were found in rat kidney, differing by a three-residue insertion in the $\beta_8\alpha_8$ barrel loop 4 [28]. The shorter LCHAO isoenzyme β1 was used in this work. The recombinant protein was expressed and purified as described [28], except that DEAE Sepharose (Amersham Biosciences) was used instead of DEAE cellulose for the second chromatographic step. Routine assays were carried out in 100 mM imidazolium/HCl buffer, pH 7.5, in the presence of 25 mM *DL*-hydroxybutyrate and 60 μM DCIP ($\varepsilon_{600} = 21\ mM^{-1}\ cm^{-1}$). For inhibition studies, the substrate used was L-mandelate, which has been found to be the most efficient substrate among the L-2-hydroxy acids tested [28]. hGOX was expressed and purified as described [29]. It was used without removing the N terminal His-tag. It was assayed in 50 mM Na+/K+ phosphate buffer, pH 7, in the presence of 10 mM glycolate and 60 μM DCIP. The Fcb2 FDH domain was expressed and purified as described in [30] with modifications [31]. Routine assays were performed in 100 mM Na+/K+ phosphate buffer, 1 mM EDTA, pH 7, with 10 mM L-lactate and 13 mM ferricyanide in cuvettes of 2 mm pathlength ($\varepsilon_{420} = 1.04\ mM^{-1}\ cm^{-1}$). For the three enzymes, assays were carried out at 30 °C using an HP8453 diode array spectrophotometer or a Uvikon 943 spectrophotometer. The enzyme concentrations were determined on the basis of the flavin concentration, using $\varepsilon_{452} = 11.7\ mM^{-1}\ cm^{-1}$, $\varepsilon_{450} = 8.6\ mM^{-1}\ cm^{-1}$ and $\varepsilon_{452} = 11\ mM^{-1}\ cm^{-1}$ for LCHAO, hGOX and the FDH domain respectively.

2.2. Screening a chemical library

The chemical library (Institut de Chimie des Substances Naturelles, CNRS, Gif-sur-Yvette) was screened using 96-well plates in a high-throughput system. The wells contained 140 μL of the relevant buffer with enzyme, substrate and electron acceptor to which were added 2 μL of inhibitor solutions in DMSO at 1 mg/ml. The substrate concentrations were 0.5 mM L-mandelate (LCHAO), 1 mM glycolate and 2 mM L-lactate. Oxalate was used as control inhibitor for LCHAO and hGOX, L-mandelate for the FDH domain. The reactions were monitored for 2 min at room temperature. Subsequently, the CCPST inhibition parameters were rigorously determined at 30 °C with the abovementioned

spectrophotometers, by varying substrates and inhibitor concentrations. The results were analyzed using several graphical representations: the double reciprocal plots, Dixon plots [32] and plots according to Cornish–Bowden [33].

2.3. Crystallography

2.3.1. Crystallization and data collection

Crystals of the LCHAO-CCPST complex were grown using the hanging drop method by mixing them in a 1:10 μM ratio at 4 °C for 2 h before crystallization. Equal volumes of 3 L each of complex solution (10 mg/ml in 100 mM Tris buffer, pH 7.5) and reservoir solution (2.8 M NaCl and 100 mM Bis–Tris, pH 6.5) were mixed and allowed to equilibrate at 23 °C for about 2 weeks. X-ray data were recorded from a single crystal at 100 K on an ADSC Quantum CCD detector at the Biocars Beamline 14-BM-C of the Advanced Photon Source, Argonne National Laboratories (Argonne, IL). Data processing, indexing, integration, and scaling were performed with the HKL2000 package [34]. The crystal was tetragonal, space group I422 with unit cell parameters $a = b = 108.4$ Å and $c = 491.7$ Å, and there are three ~43 kDa protomers per asymmetric unit. The data collection statistics are summarized in Table 1.

2.3.2. Structure determination and refinement

The complex structure was solved by molecular replacement with MOLREP from the ccp4 package [35] using as a starting model the coordinates of subunit A from the ligand-free structure (PDB ID code 1TB3 [19]), with all cofactor and solvent molecules omitted. Rigid body refinement and several cycles of positional, temperature factor and simulated annealing refinement, followed by interactive model building and automatic solvent placement with manual examination, were carried out. Model building and analysis of the structure were carried out on a Silicon Graphics workstation using Turbo-Frodo [36]. The refinement and electron density calculations were carried out using CNS [37] and 5% of the reflections were selected randomly and set aside as a test set for cross validation [38]. Non-crystallographic symmetry (NCS) restraints were applied to the three protein molecules in the asymmetric unit (with NCS weights set to 300 for both main and side chain atoms). In the final cycle of refinement, the NCS restraints were removed. The final R_{cryst} and R_{free} are 0.185 and 0.203, with rmsd from ideal values of 0.013 Å for bond lengths and 1.8° for bond angles, respectively. The final model consists of 1001 residues which include 14 residues with two alternate conformations, 3 FMN, 3 CCPST and 1104 water molecules. The refinement and model parameters are listed in Table 1.

Table 1
Summary of data collection and refinement for the complex of LCHAO and the inhibitor CCPST.

Sample name	LCHAO-CCPST complex
Data collection	
Wavelength (Å)	0.9
Space group	I422
No. mol. per asymmetric unit	3
Res. range (last shell) (Å)	40–1.35 (1.40–1.35)
No. observations	3,495,344
Unique observations	311,329
Completeness (last shell) (%)	98.5 (94.8)
R_{merge}[a] (last shell) (%)	8.7 (33.4)
$I/\sigma(I)$[b] (last shell)	26.6 (2.6)
Refinement	
Resolution (Å)	40–1.35
$\|F\|/\sigma(\|F\|)$	>0
R_{cryst}[c]	0.185
R_{free}[d]	0.203
Reflections (working/test)	295,849/15,480
Protein atoms	7779
Water molecules	1104
FMN atoms	93
CCPST atoms	48
Rmsd bond lengths[e] (Å)	0.013
Rmsd angles[e] (°)	1.8
Rms ΔB (Å^2) (mm/ms/ss)[f]	1.60/2.15/3.22
<B> protein (Å^2)	19.5
<B> water molecules (Å^2)	29.2
<B > FMN	11.4
<B > CCPST	18.0
Residues with the alternate conformers (molecule numbers)	Met54 (ABC), Ser81 (ABC), Ile104 (ABC), Thr158 (AC), Cys297 (ABC)
Ramachandran plot (%)[g]	
Allowed region	98.7
Generously allowed region	1.2
Disallowed region	0.1
PDB entry	3SGZ

[a] $R_{merge} = \sum_h \sum_i |I(h) - I_i(h)| / \sum_h \sum_i I_i(h)$, where $I_i(h)$ and $I(h)$ are the ith and mean measurements of reflection h.
[b] $I/\sigma(I)$ is the average signal to noise ratio for merged reflection intensities.
[c] $R = \Sigma_h$Fo − Fc/Σ_hFo, where Fo and Fc are the observed and calculated structure factor amplitudes of reflection h.
[d] R_{free} is R for the test reflection data set.
[e] Root-mean-squared deviation (Rmsd) from ideal bond lengths and angles and Rmsd in B-factors of bonded atoms.
[f] Mm, main chain to main chain; ms, main chain to side chain, ss, side chain to side chain.
[g] The Ramachhandran plot was computed using PROCHECK [35]; the one residue in the disallowed region is Ser350 of chain A, which may be somewhat poorly ordered.

2.4. Theoretical calculations

In order to obtain insight concerning the most stable protonation state of TACA and CDST (Fig. 1), the structure of an analogue carrying a methyl group on the sulfur atom instead of the hydrophobic substituents (4-carboxy-5-methylsulfanyl-1,2,3-triazole) was analyzed using the DFT (B3LYP/6-31G*) method. Separate geometry optimization *in vacuo* for the N1 and N3 protomers was carried out assuming a negative charge and a singlet spin state.

3. Results

3.1. Enzymatic characterization of the inhibitor

A chemical library of about 3000 compounds was screened for LCHAO, hGOX and FDH domain inhibitors, as described in Materials and Methods. Among several hits, CCPST drew our attention, because of its overall similarity with TACA (Fig. 1), an inhibitor which had been crystallized in complex with sGOX [26]. Under the conditions of the enzymatic tests used in the screening, the CCPST IC_{50} was on the order of a few μM for the three enzymes. Kinetic analyses using double reciprocal plots showed that the inhibition was not simply competitive for any of the enzymes. The inhibition type was confirmed by plots according to Dixon [32] and to Cornish–Bowden [33]; graphical results are presented as supplemental data (Figure S1). Using the classical terminology, LCHAO and hGOX inhibition was non-competitive, with $K_i = K_i' = 3.6 \pm 0.1$ μM for the former and $K_i = K_i' = 4.5 \pm 1.5$ μM for the latter. For the Fcb2 FDH domain, inhibition was uncompetitive, with $K_i = 6 \pm 3$ μM. During the FDH catalytic cycle in the presence of ferricyanide as acceptor, the flavin passes through three redox states: oxidized, one-electron reduced (semiquinone) and two-electron reduced (hydroquinone). It may also be the case for hGOX and LCHAO with DCIP as acceptor, but not necessarily since the latter can also act as a two-electron acceptor. By analogy with more detailed kinetic results obtained with several inhibitors of the FDH domain [31], the results for LCHAO and hGOX suggest that the inhibitor binds to the active site not only when the flavin is

oxidized, but also when it is reduced, in the latter case inhibiting enzyme reoxidation. With respect to the results for the Fcb2 FDH domain, uncompetitive inhibition by pyruvate at high concentrations has been observed for the *Hansenula anomala* Fcb2 [39]. The authors analyzed their results as indicating a binding of pyruvate to the active site when the flavin is in the oxidized and the semiquinone state. Further kinetic studies would be needed in order to clarify the situation with respect to the inhibition by CCPST, but these are outside the scope of the present work.

3.2. Structure of the CCPST complex

The complex of LCHAO with the CCPST inhibitor crystallizes with three independent protomers in the asymmetric unit. One of these protomers (chain A) forms an exact crystallographic octamer with 222 symmetry while the other protomers (chains B and C) each form tetramers with exact circular 4-fold crystallographic symmetry that pack together to form an octamer with non-crystallographic 2-fold symmetry. Each of the three protomers is folded into a $\beta_8\alpha_8$ barrel motif, closely similar to all other members of the FMN-containing hydroxy acid-oxidizing enzyme families, with the isoalloxazine ring and the associated CCPST inhibitor located among peptide loops at the C-terminal end of the β barrel.

Protomers A and C each consist of 335 residues, from 1 to 181 and 198–351 with a portion of the loop 4 segment (that connects strand β4 to helix α4), residues 182–197, and the C-terminal residue, 352, missing from the electron density map; protomer B is the same except that residues 350 and 351 are also missing from the C-terminus. Protomers A and C are most similar, displaying an rms deviation of 0.27 Å for equivalent Cα atoms of all 335 residues. The largest deviation between these protomers occurs for residues 207–217 where the rmsd is 1.11 Å. This segment is well ordered in both protomers and corresponds to helix α_4 in which a crystal packing contact between the two protomers is located. Protomer B differs to a greater extent from protomers A and C, showing a rmsd of 0.46 Å with respect to each of them. The largest difference, contained in segment 130–140 that contains helix α_3, differs from those of protomers A and C by 1.16 and 1.29 Å, respectively. The segment is on the protein surface and makes minimal crystal packing contacts.

3.3. Comparison of the acetate and CCPST complexes of LCHAO

The structure of the acetate complex of LCHAO was determined at 2.3 Å resolution and refined with 8 independent protomers in the unit cell that were restrained by non-crystallographic symmetry. The polypeptide chain could be traced from residues 1–176 and 202–349 in all 8 subunits; in addition, all or portions of a short intervening segment, tentatively identified as residues "181–188", could be visualized in 7 of the subunits although the electron density was quite weak. Comparison of the acetate and CCPST complexes show an rmsd of 0.26 $Å^2$ for 318 equivalent Cα atoms, calculated with the poorly ordered "181–188" segment in the acetate complex omitted.

Since the disorder of the loop 4 region is localized to different regions in the acetate and the CCPST complexes, a comparison of their ordered and partially ordered segments provides some insight into the nature of its configuration in solution. The acetate and CCPST models are essentially congruent everywhere over the residue ranges 1–170 and 202–349 (Fig. 2). However, segment 171–176 of the acetate complex forms an extended chain while segment 171–181 of the CCPST complex diverges to form a partially helical motif that is located about 5 Å away. At the C-terminal end of the missing segment, the CCPST complex picks up again at residue 198 as an extended chain (Fig. 2), which leads to residue 203, which is positioned very close to residue 203 of the acetate complex. Residue 202 of the acetate complex, the first identified residue after the C-terminal end of the loop 4 gap, is about 2.9 Å from residue 202 of the CCPST complex. Finally, the poorly ordered segment of the acetate complex ("181–188") is seen to lay over the front face of the active site pocket stretching from its N-terminus, at a position near the N terminal ends of helices α_1 and α_2, to its C-terminus close to residue 198 of the CCPST complex (Fig. 2). The close juxtaposition of these two segments suggests that the one from the acetate complex could be renumbered as "191–198", although its weak electron density in the acetate complex provides only limited support for this hypothesis.

The interactions of the flavin ring with the protein main and side chain atoms in the CCPST complex are virtually the same as in the original acetate complex (PDB code 1TB3) and in the hGOX-CCPST complex (PDB code 2W0U) (Table S1). The extended peptide

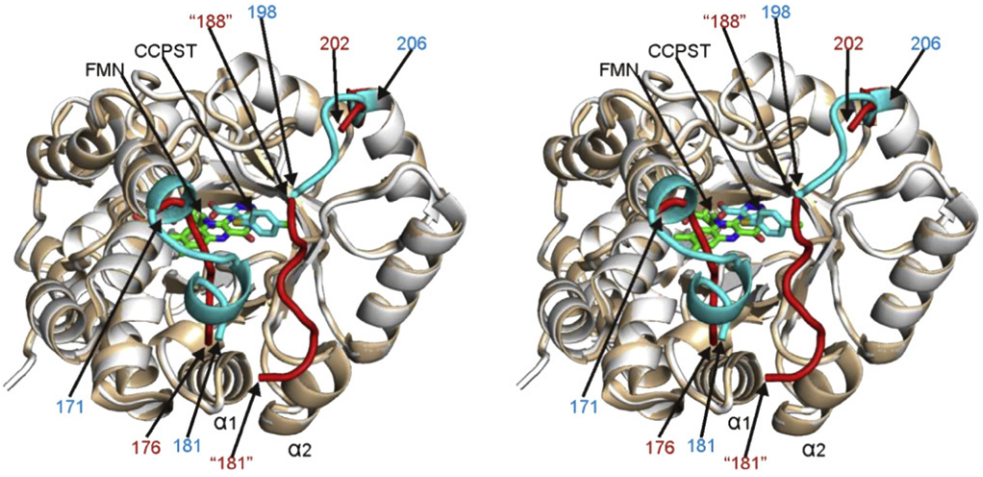

Fig. 2. Cartoon drawing of the superimposed acetate and CCPST complexes of LCHAO. The two complexes, both depicting chains A, are shown in wheat and light grey, respectively, except for their loop 4 segments, which are shown in red and cyan, respectively. The red segments and segment labels (acetate complex) correspond to residues 171–176, 202–206 and (as defined previously [19]) "181–188". The cyan segments and segment labels (CCPST complex) correspond to residues 171–182 and 198–206. The FMN and CCPST molecules are shown as stick figures with atoms O coloured red, N blue, S yellow, Cl green and, for FMN, C green and, for CCPST, C cyan. For clarity, the acetate ligand is not shown. The molecule is viewed from the top of the $\beta_8\alpha_8$ barrel into the active site cavity. (For interpretation of the references to colour in this figure legend, the reader is referred to the web version of this article.)

Table 2
Hydrophobic interactions between CCPST and the flavin ring in LCHAO and hGOX.

LCHAO			hGOX		
CCPST atom	Flavin atom	Dist. (Å)[a]	CCPST atom	Flavin atom	Dist. (Å)[b]
–	–	–	N1	O4	3.18
N1	C4	3.58	N1	C4	3.35
–	–	–	N2	C4	3.27
N2	C4a	3.39	N2	C4a	3.29
C8	N5	3.48	C8	N5	3.46
C9	N5	3.58	C9	N5	3.50
C9	C5a	3.50	C9	C5a	3.49
O1	C5a	3.51	O1	C5a	3.49
O1	C9	3.50	–	–	–
O2	C6	3.65	O2	C6	3.45

[a] Average of three molecules in the asymmetric unit of LCHAO.
[b] Average of four molecules in the asymmetric unit of hGOX.

chain that lies on its *re* side is engaged in hydrogen bonds with the flavin O2′ and N5 atoms *via* the Pro76 carbonyl oxygen and the Ala78 NH, respectively. Hydrogen bonds are also formed between conserved side chains and FMN O2, N3 and O4. In addition, NZ of Lys223 interacts with N1, O2 and the ribityl O2′ (Table S1).

3.4. Active site of the LCHAO-CCPST complex

The atoms of the 5-membered ring and carboxylate group of CCPST lie nearly in a plane, as do the atoms of the flavin ring. Their planes are nearly parallel, with the atoms N2, N1, C8, C9, O1 and O2 of CCPST located almost directly above atoms C4, C4a, N5, C5a, C9 and C6 of the *si* face of the isoalloxazine ring at distances of about 3.3–3.5 Å (Table 2).

CCPST is involved in seven ionic or hydrogen bonding interactions with protein side chains (Fig. 3, Table 3). The CCPST carboxylate oxygens form hydrogen bonds with Arg250 NE and NH2, and an electrostatic interaction with Arg164. In addition, both O1 and N2 interact with His247 NE2. Finally, N1 receives a hydrogen bond from the Tyr129 OH. The chlorophenyl ring of CCPST extends away from the active site toward the protein surface and is enveloped by the aliphatic and aromatic portions of the side chains of Phe79, Tyr107 and Leu161 as well as residues Ala198 and Phe199 that are situated immediately after the missing loop 4 segment of the molecule.

The nitrogen and oxygen atoms of CCPST are all serving as hydrogen bond acceptors in their interactions with the protein side chains. In the case of the ring nitrogen atoms of CCPST, neither can be protonated since they are joined by a double bond and the ring is essentially planar, so that a proton must reside on atom NE2 of His247. Consequently His247 must be doubly protonated, since its other ring nitrogen, ND1, is hydrogen bonded to the side chain of Asp157 (Fig. 3). The distances of His247 NE2 to CCPST atoms N2 and O1 are both under 3 Å indicating that this hydrogen bond is bifurcated, as indicated by the red dashed lines in Fig. 3. In the unliganded enzyme, this active site histidine, the catalytic base, is neutral [40].

When the binding of the acetate and CCPST ligands are compared, the acetate group is found to lie approximately in the plane formed by the 5-membered ring and carboxylate group of CCPST, but the carboxylate group of the acetate is oriented differently, by approximately a 120° rotation in the plane from that in the CCPST complex, with its oxygen atoms interacting with the side chains of Arg164, His247 and Tyr129. The binding of CCPST is more similar to the binding of the product pyruvate in flavocytochrome b_2 with the FMN in the semiquinone state [25,41] and the substrate octanoic acid in reduced mandelate dehydrogenase [42].

3.5. Comparison of the CCPST binding in human glycolate oxidase and rat LCHAO

The CCPST inhibitor interactions with the flavin ring are nearly identical in human GOX and in rat LCHAO (Table 2). The flavin and inhibitor rings are nearly parallel to each other and separated to the same extent (3.3–3.5 Å). However, the hydrogen bonding interactions of CCPST in the two proteins are somewhat different (Table 3). In both proteins N1 of CCPST forms an H bond to a tyrosine side chain, Tyr129/132. In both proteins the carboxylate oxygens are hydrogen bonded to Arg250/263 NE and NH2. But the distance between these oxygens and the Arg164/167 nitrogens is shorter in the LCHAO complex than in the hGOX complex (Table 3, Fig. 4) so that in the latter case the ionic interaction must be weaker. In addition, O2 forms an H bond with hGOX Tyr26, which is replaced by Phe23 in LCHAO. In the latter, as a compensation, O1 of CCPST shares with N2 the bifurcated hydrogen bond from H247 NE2,

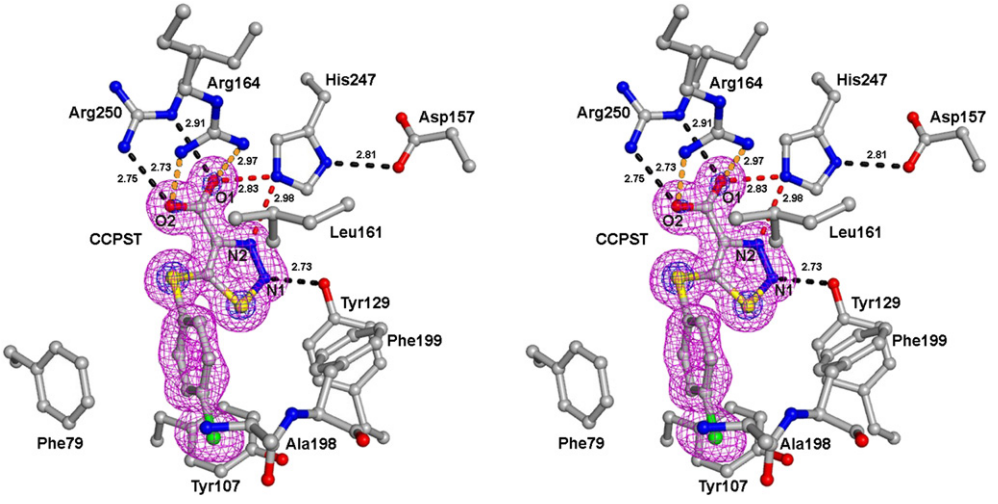

Fig. 3. Hydrogen bonding, ionic and hydrophobic interactions of CCPST in molecule A of LCHAO, superimposed on its electron density, with nearby side chains of LCHAO. The electron density is contoured at the 1 sigma (magenta) and the 7 sigma (blue contours) within a 1.5 Å radius of all atoms of CCPST. The direct H bonds from the side chains of Tyr129 and Arg250 to CCPST and between His247 and Asp157 are shown as black dashed lines with the distances. The ionic interactions between Arg164 and CCPST are shown as orange dashed lines. The bifurcated H bond from His247 to atoms O1 and N2 is shown as red dashed lines. The side chains that surround the chlorophenyl moiety of CCPST and form a hydrophobic cage, Phe79, Tyr107, Leu161, Ala198 and Phe199, are also shown. The atoms C are coloured grey, N blue, O red, S yellow and Cl green. (For interpretation of the references to colour in this figure legend, the reader is referred to the web version of this article.)

Table 3
Polar CCPST–protein interactions in LCHAO and hGOX.

LCHAO			hGOX		
CCPST atom	Protein atom	Dist. (Å)[a]	CCPST atom	Protein atom	Dist. (Å)[b]
N1	Tyr129 OH	2.73	N1	Tyr132 OH	2.92
N2	His247 NE2[c]	2.98	N2	His260 OH	2.92
O1	Arg250 NE	2.91	O1	Arg263 NE	2.72
O1	Arg164 NH2	2.97[d]	O1	Arg167 NH2	3.29[e]
O1	His247 NE2[c]	2.83	–	–	–
O2	Arg250 NH2	2.75	O2	Arg263 NH2	2.76
O2	Arg164 NH1	2.73[d]	O2	Arg167 NH1	3.25[e]
–	–	–	O2	Tyr26 OH	3.06
Cl	Ala198 O	3.46	Cl	Trp110 NE	2.95

[a] Average of three molecules in the asymmetric unit of LCHAO.
[b] Average of four molecules in the asymmetric unit of hGOX.
[c] Bifurcated hydrogen bond with atoms N2, O1 of CCPST.
[d] In LCHAO the distance is close but the angle poor for hydrogen bond formation to oxygen atoms O1 and O2 of CCPST.
[e] In hGOX the distance is longer and the angle poor for hydrogen bond formation to oxygen atoms O1 and O2 of CCPST.

while in hGOX only N2 interacts with His260. The differences in the hydrogen bonding arrangements of CCPST in the two enzymes appears to be caused principally by the replacement of Tyr26 in hGOX with Phe23 in LCHAO.

The chlorophenyl ring of CCPST points approximately in the same direction in the two proteins, although the benzene ring is twisted by about 90° between the two structures. It forms weak hydrophobic interactions with surrounding main and side chain atoms which are similar in their properties. One exception is the chlorine atom which forms a hydrogen bond with atom NE of Trp118 in hGOX (Table 3) but a weaker interaction with the carbonyl oxygen of Ala198 in LCHAO.

4. Discussion

4.1. Structural comparisons, the loop 4 case

The structure of the complex presented in this work has been solved to 1.3 Å resolution, a better resolution than for most members of this family of L-2-hydroxy acid-oxidizing flavoenzymes, and in particular than the first structure of LCHAO in complex with acetate at 2.3 Å. Nevertheless, these two structures superimpose very well, as discussed above, except for certain residues within and in the vicinity of the active site. The most remarkable alterations are observed in loop 4. In many structures of family members, between 10 and 30 residues of loop 4 are disordered and invisible. This loop is fully defined in some subunits of the structures of lactate oxidase [23,43,44], as well as in the structure of the chimeric mandelate dehydrogenase, in which the original loop has been replaced by that of sGOX [24]. It is also fully defined in two structures of hGOX in complex with the small ligands sulfate and glyoxylate (the latter is the product of the reaction). But binding of the larger ligand CDST (Fig. 1) induced disorder in hGOX loop 4 [21]. When visible, loop 4 occludes the active site from the solvent, but forms few if any direct interactions with the ligand. In the hGOX case, the disordering is caused by the suppression of an H bond between a loop 4 residue and W110, a residue whose indole ring changes orientation upon CDST binding [21]. In the LCHAO case with acetate bound, even though the latter is a small molecule (picked up from the mother liquors), only a segment of eight residues can be tentatively identified between two gaps from positions 177 to 201. But, in contrast, binding of CCPST induced a conformational change in the visible part and an ordering of a few more residues (Fig. 2). Thus, the present structure provides one more example of the plasticity of loop 4 in this enzyme family, and of the way its structure can be modulated by what is present in or around the active site, as discussed for example in [21,41]. At the functional level, LCHAO isozyme β2, with three additional residues (VRK) between positions 188 and 189, induces small differences in the kinetic parameters for some substrates and inhibitors [28]. Also, selective proteolysis of loop 4 in Fcb2 significantly alters the kinetic parameters for lactate oxidation, suggesting an influence on the structure of active site residues and/or on ligand binding [45]. In any case, all these results suggest that loop 4 could play a role in the selectivity of inhibitors, but an unpredictable role.

CCPST, CDST and TACA (Fig. 1) all have a carboxylate attached to a five-membered ring and a hydrophobic substituent. Notwithstanding the replacement of a nitrogen with a sulfur in CCPST, the

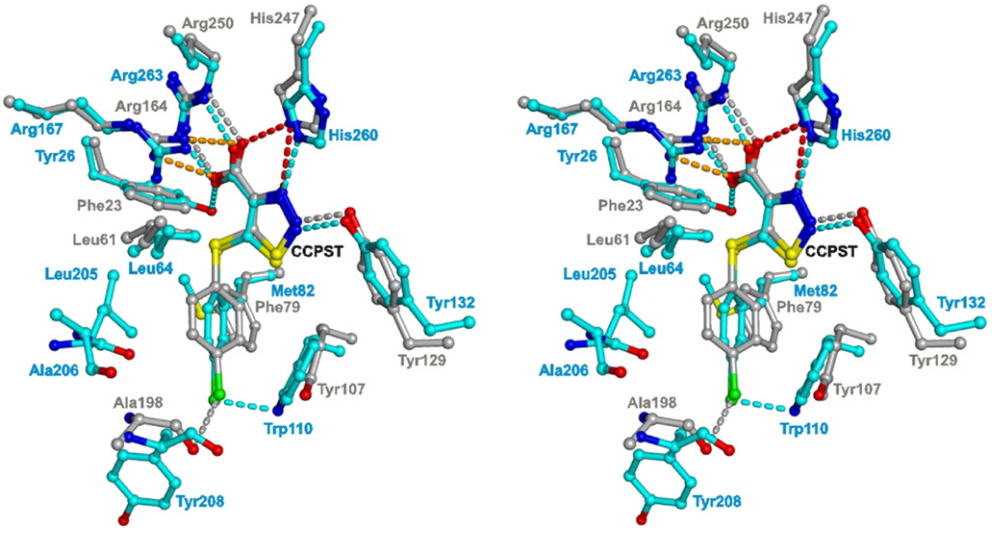

Fig. 4. Comparison of the CCPST interactions with molecules A of LCHAO and of hGOX. The atom colouring is O red, S yellow, Cl green, N blue for both molecules. For LCHAO, the atoms C are grey and for hGOX cyan, respectively, as are the residue identifiers for the two structures. The hydrogen bonding interactions are shown as dashed lines in cyan for hGOX and in grey for LCHAO, except for the bifurcated hydrogen bond involving His247 which is in red. The ionic interactions between Arg164 and CCPST in LCHAO are shown as orange dashed lines. (For interpretation of the references to colour in this figure legend, the reader is referred to the web version of this article.)

carboxylate and the ring nitrogen atoms of these three compounds bind to invariant catalytic residues in a very similar fashion. The carboxylates all interact with the same two arginines, one of the ring nitrogens with the histidine, and the other nitrogen with one of the tyrosines. In the GOX structures, one of the carboxylate oxygens of the three inhibitors forms in addition an H bond with the other active site tyrosine which is replaced in LCHAO with a phenylalanine. In the latter case, for CCPST, the loss of this interaction appears to be compensated by the participation of the other carboxylate oxygen in a bifurcated hydrogen bond from the histidine. In contrast, the hydrophobic substituents of the rings, which are different for the three compounds, form diverse interactions with non conserved residues, some of which have been shown by site-directed mutagenesis to be involved in specificity [46]. They also induce movements in part of loop 4, as well as the reorientation of some side chains that do not belong to this loop, such as for example in hGOX Trp110 (loop 2), Tyr134 (loop-3), Tyr208 (loop 4) (in sGOX Trp108, Tyr131 and Tyr202, respectively) (*20*, *25*, *26*). In LCHAO, the homologous residues are Tyr107, Lys131 and Val191; the orientation of the Tyr107 aromatic ring is only slightly different between the acetate complex [19] and the present complex, and Val191 is invisible in both cases. In the complex with CCPST, the most conspicuous alterations pertain to the Leu161 side chain (L164 in hGOX) and other elements of loop 4 with different degrees of order or disorder, as described above.

4.2. Protonation state of the active site histidine, role in ligand binding

The K_d value of TACA for sGOX is reported to be 16 nM [26] and that of CDST for hGOX ~15 nM [21], while those of CCPST for hGOX and rat LCHAO are about two orders of magnitude higher, as reported above. How can one rationalize this difference? One difference between TACA and CDST, on the one hand, and CCPST, on the other hand, is the flexibility of the hydrophobic substituents in the former inhibitors, which may facilitate adaptation of the protein structure in the mobile region, compared to the rigidity of the chlorophenyl ring in CCPST. Nevertheless, although the ring environment is not identical in hGOX and LCHAO (Fig. 4), the CCPST dissociation constants are practically identical between the two enzymes. Another difference lies in the replacement of a ring nitrogen atom (N1 of CDST and TACA, Fig. 1) by a sulfur atom. This may not be important *per se*, as the atoms at this position do not appear to make close contacts with protein atoms. But this N/S replacement makes it clear that CCPST cannot carry a proton on one of the ring nitrogen atoms in contrast with TACA and CDST. As discussed above and by Bourhis et al. [27], the binding of CCPST to hGOX and LCHAO requires that the active site histidine picks up a proton from solution in order to form a hydrogen bond to CCPST N2 and thus undergoes a pK_a change. On the other hand, CDST and TACA each carry a ring-borne proton. In Fig. 1, this proton resides on the N1 of CDST, as in [21], and on N3 of TACA, as in [26]. Interestingly, theoretical calculations on a simple model of TACA and CDST, with the hydrophobic substituent replaced with a methyl group, suggest that the protomer with the proton on N3 would be more stable than the other one by about 15 kcal/mol *in vacuo* (see Materials and Methods). Thus, the proton required for the H bond of TACA and CDST with the respective histidines would likely in both cases reside on N3 and be available for binding, which would be energetically less costly than having to protonate this active site histidine as in the case of binding CCPST. The greater energy cost required to protonate this histidine upon binding CCPST may contribute substantially to its weaker binding compared to the other two inhibitors. The present results suggest that, in order to improve the affinity, one should look for molecules carrying a protonated atom at a position β to a carboxylate, among other hydrogen bonding capacities.

LCHAO and GOX are isozymes. In the human genome, no genes coding for other homologues have been identified [17,18]. The sequence identity between rat LCHAO and hGOX is 46.4%, that between the two human isozymes is 73.6%. In both comparisons, the identity is much lower in the loop 4 sequence, with the latter being longer by ten residues in glycolate oxidase. The absence of specificity of CCPST between rat LCHAO and hGOX suggests that in the search for inhibitors of either human enzyme for potential therapeutic uses, one should investigate both enzymes in parallel. Yet the quest is probably not hopeless, since in our screening of about 3000 compounds, a few hits did discriminate between rat LCHAO and hGOX (C. Vignaud and F. Lederer, unpublished experiments).

Acknowledgements

This study was made possible by a fellowship from the Institut de Chimie des Substances Naturelles (CNRS, Gif-sur-Yvette) to C. V. The authors are grateful to Professor J.-Y. Lallemand for his interest in and his support to the project.

Appendix. Supplementary material

Supplementary data associated with this article can be found, in the online version, at doi:10.1016/j.biochi.2012.02.003.

References

[1] M. Blanchard, D.E. Green, V. Nocito, S. Ratner, L-amino acid oxidase of animal tissue, J. Biol. Chem. 155 (1944) 421–440.
[2] M. Blanchard, D.E. Green, V. Nocito-Carroll, S. Ratner, L-hydroxy acid oxidase, J. Biol. Chem. 163 (1946) 137–144.
[3] M. Nakano, Comparison of the enzyme oxidizing thyroid hormone with L-amino acid oxidase, Biochim. Biophys. Acta 92 (1964) 472–481.
[4] J.L. Stevens, P.B. Hatzinger, P.J. Hayden, Quantitation of multiple pathways for the metabolism of nephrotoxic cysteine conjugates using selective inhibitors of L-α-hydroxy acid oxidase (L-amino acid oxidase) and cysteine conjugate ß-lyase, Drug Metab. Dispos. 17 (1989) 297–303.
[5] J.L. Stevens, J.D. Robbins, R.A. Byrd, A purified cysteine conjugate ß-lyase from rat kidney cytosol. Requirement for an α-keto acid or an amino acid oxidase for activity and identity with soluble glutamine transaminase, J. Biol. Chem. 261 (1986) 15529–15537.
[6] E.J. Brush, G.A. Hamilton, Thiol-glyoxylate adducts as substrates for rat kidney L-α-hydroxy acid oxidase, Biochem. Biophys. Res. Commun. 103 (1981) 1194–1200.
[7] S. Gunshore, E.J. Brush, G.A. Hamilton, Equilibrium constants for the formation of glyoxylate thiohemiacetals and kinetic constants for their oxidation by O_2 catalyzed by L-hydroxy acid oxidase, Bioorg. Chem. 13 (1985) 1–13.
[8] H. Ozasa, S. Horikawa, K. Ota, Methylguanidine synthase from rat kidney is identical to long-chain L-2-hydroxy acid oxidase, Nephron 68 (1994) 279.
[9] T. Yokozawa, N. Fujitsuka, H. Oura, T. Akao, K. Kobashi, K. Ienaga, K. Nakamura, M. Hattori, Purification of methylguanidine synthase from the rat kidney, Nephron 63 (1993) 452–457.
[10] P. De Deyn, B. Marescau, W. Lornoy, I. Becaus, I. Van Leuven, L. Van Gorp, A. Lowenthal, Serum guanidino compound levels and the influence of a single hemodialysis in uremic patients undergoing maintenance hemodialysis, Nephron 45 (1987) 291–295.
[11] P.P. De Deyn, R. D'Hooge, P.P. Van Bogaert, B. Marescau, Endogenous guanidino compounds as uremic neurotoxins, Kidney Int.(Suppl. 78) (2001) S77–S83.
[12] K. Nakamura, K. Ienaga, Creatol (5-hydroxycreatinine), a new toxin candidate in uremic patients, Experientia 46 (1990) 470–472.
[13] T. Yokozawa, N. Fujitsuka, H. Oura, K. Ienaga, K. Nakamura, Comparison of methylguanidine production from creatinine and creatol *in vivo*, Nephron 58 (1991) 125–126.
[14] C.J. Danpure, Primary hyperoxaluria, in: C.R. Scriver, A.L. Beaudet, W.S. Sly, D. Valle, B. Childs, K.W. Kinzler, B. Vogelstein (Eds.), The Metabolic and Molecular Bases of Inherited Disease, McGrax-Hill, New York, 2001, pp. 3323–3367.
[15] R.P. Holmes, Pharmacological approaches in the treatment of primary hyperoxaluria, J. Nephrol. 11 (Suppl. 1) (1998) 32–35.
[16] A. Belmouden, K.H.D. Lê, F. Lederer, H.-J. Garchon, Molecular cloning and nucleotide sequence of cDNA encoding rat kidney long-chain L-2-hydroxy acid oxidase. Expression of the catalytically active recombinant protein as a chimaera, Eur. J. Biochem. 214 (1993) 17–25.

[17] J.M. Jones, J.C. Morrell, S.J. Gould, Identification and characterization of HAOX1, HAOX2, and HAOX3, three human peroxisomal 2-hydroxy acid oxidases, J. Biol. Chem. 275 (2000) 12590–12597.
[18] J.M. Jones, J.C. Morrell, S.J. Gould, Identification and characterization of HAOX1, HAOX2, and HAOX3, three human peroxisomal 2-hydroxy acid oxidases, J. Biol. Chem. 275 (2004) 35122.
[19] L.M. Cunane, J.D. Barton, Z.-w. Chen, K.H.D. Lê, D. Amar, F. Lederer, F.S. Mathews, Crystal structure analysis of recombinant rat kidney long-chain α-hydroxy acid oxidase, Biochemistry 44 (2005) 1521–1531.
[20] Y. Lindqvist, Refined structure of spinach glycolate oxidase at 2 Å resolution, J. Mol. Biol. 209 (1989) 151–166.
[21] M.S. Murray, R.P. Holmes, W.T. Lowther, Active site and loop 4 movements within human glycolate oxidase: implications for substrate specificity and drug design, Biochemistry 47 (2008) 2439–2449.
[22] K. Maeda-Yorita, K. Aki, H. Sagai, H. Misaki, V. Massey, L-lactate oxidase and L-lactate monooxygenase: mechanistic variations on a common structural theme, Biochimie 77 (1995) 631–642.
[23] Y. Umena, K. Yorita, T. Matsuoka, A. Kita, K. Fukui, Y. Morimoto, The crystal structure of L-lactate oxidase from *Aerococcus viridans* at 2.1 Å resolution reveals the mechanism of strict substrate recognition, Biochem. Biophys. Res. Commun. 350 (2006) 249–256.
[24] N. Sukumar, A.R. Dewanti, B. Mitra, F.S. Mathews, High resolution structures of an oxidized and reduced flavoprotein: the water switch in a soluble form of mandelate dehydrogenase, J. Biol. Chem. 279 (2004) 3749–3757.
[25] Z.-x. Xia, F.S. Mathews, Molecular structure of flavocytochrome b_2 at 2.4 Å resolution, J. Mol. Biol. 212 (1990) 837–863.
[26] K. Stenberg, Y. Lindqvist, Three-dimensional structures of glycolate oxidase with bound active-site inhibitors, Protein Sci. 6 (1997) 1009–1015.
[27] J.M. Bourhis, C. Vignaud, N. Pietrancosta, F. Guéritte, D. Guénard, F. Lederer, Y. Lindqvist, Structure of human glycolate oxidase in complex with the inhibitor 4-carboxy-5-[(4-chlorophenyl)sulfanyl]-1, 2, 3-thiadiazole, Acta Cryst. Sect. F 65 (2009) 1246–1253.
[28] A. Belmouden, F. Lederer, The role of a ß barrel loop 4 extension in modulating the physical and functional properties of long-chain 2-hydroxy acid oxidase isozymes, Eur. J. Biochem. 238 (1996) 790–798.
[29] C. Vignaud, N. Pietrancosta, E.L. Williams, G. Rumsby, F. Lederer, Purification and characterization of recombinant human liver glycolate oxidase, Arch. Biochem. Biophys. 465 (2007) 410–416.
[30] A. Balme, C.E. Brunt, R. Pallister, S.K. Chapman, G.A. Reid, Isolation and characterization of the flavin-binding domain of flavocytochrome b_2, expressed independently in *Escherichia coli*, Biochem. J. 309 (1995) 601–605.
[31] N. Cénas, K.H.D. Lê, M. Terrier, F. Lederer, Potentiometric and further kinetic characterization of the flavin-binding domain of *Saccharomyces cerevisiae* flavocytochrome b_2. Inhibition by anion binding in the active site, Biochemistry 46 (2007) 4661–4670.
[32] M. Dixon, The determination of enzyme inhibitor constants, Biochem. J. 55 (1953) 170–171.
[33] A. Cornish-Bowden, A simple graphical method for determining the inhibition constants of mixed, uncompetitive and non-competitive inhibitors, Biochem. J. 137 (1974) 143–144.
[34] Z. Otwinowski, W. Minor, Processing of x-ray diffraction data collected by oscillation methods, Methods Enzymol. 276 (1997) 307–326.
[35] The CCP4 suite: programs for protein crystallography, Acta Cryst. Sect. D 50 (1994) 760–763.
[36] A. Roussel, C. Cambillau, Turbo Frodo, in Silicon Graphics geometry Partners Directory, Silicon Graphic, Mountain View, CA., USA, 1989, pp. 77–78.
[37] A.T. Brünger, P.D. Adams, G.M. Clore, W.L. DeLano, P. Gros, R.W. Grosse-Kunstleve, J.S. Jiang, J. Kuszewski, M. Nilges, N.S. Pannu, R.J. Read, L.M. Rice, T. Simonson, G.L. Warren, Crystallography & NMR system: a new software suite for macromolecular structure determination, Acta Cryst. D 54 (1998) 905–921.
[38] A.T. Brünger, Free R-value: a novel statistical quantity for assessing the accuracy of crystal structures, Nature (London) 355 (1992) 472–475.
[39] M. Tegoni, J.M. Janot, F. Labeyrie, Inhibition of L-lactate cytochrome *c* reductase – flavocytochrome b_2 – by product binding to the semiquinone transient: loss of reactivity towards monoelectronic acceptors, Eur. J. Biochem. 190 (1990) 329–342.
[40] K.S. Rao, F. Lederer, About the pK_a of the active-site histidine in flavocytochrome b_2 (yeast L-lactate dehydrogenase), Protein Sci. 7 (1998) 1531–1537.
[41] L.M. Cunane, J.D. Barton, Z.W. Chen, F.E. Welsh, S.K. Chapman, G.A. Reid, F.S. Mathews, Crystallographic study of the recombinant flavin-binding domain of Baker's yeast flavocytochrome b_2: comparison with the intact wild-type enzyme, Biochemistry 41 (2002) 4264–4272.
[42] N. Sukumar, A. Dewanti, A. Merli, G.L. Rossi, B. Mitra, F.S. Mathews, Structures of the G81A mutant form of the active chimera of (*S*)-mandelate dehydrogenase and its complex with two of its substrates, Acta Cryst. Sect. D 65 (2009) 543–552.
[43] I. Leiros, E. Wang, T. Rasmussen, E. Oksanen, H. Repo, S.B. Petersen, P. Heikinheimo, E. Hough, The 2.1 Å structure of *Aerococcus viridans* L-lactate oxidase (LOX), Acta Cryst. Sect. F 62 (2006) 1185–1190.
[44] S.J. Li, Y. Umena, K. Yorita, T. Matsuoka, A. Kita, K. Fukui, Y. Morimoto, Crystallographic study on the interaction of L-lactate oxidase with pyruvate at 1.9 Å resolution, Biochem. Biophys. Res. Commun. 358 (2007) 1002–1007.
[45] R. Ghrir, F. Lederer, Study of a zone highly sensitive to proteases in flavocytochrome b_2 from Saccharomyces cerevisiae, Eur. J. Biochem. 120 (1981) 279–287.
[46] K. Stenberg, T. Clausen, Y. Lindqvist, P. Macheroux, Involvement of Tyr24 and Trp108 in substrate binding and substrate specificity of glycolate oxidase, Eur. J. Biochem. 228 (1995) 408–416.